
Breakup dynamics of a neutron-halo projectile on heavy target at deep sub-barrier energies

B. MUKERU^{1,2}, T. SITHOLE¹ and LAURO TOMIO^{3,4(a)}

¹ *Department of Physics, University of South Africa - Private Bag X6, Florida 1710, Johannesburg, South Africa*

² *Université Pédagogique Nationale, Av. de la Libération, P.O. Box 8815, Kinshasa, Democratic Republic of Congo*

³ *Centro Internacional de Física, Instituto de Física, Universidade de Brasília, 70910-900, Brasília, DF, Brazil*

⁴ *Instituto de Física Teórica, Universidade Estadual Paulista, 01140-070 São Paulo, SP, Brazil*

E-mail: mukerb1@unisa.ac.za, sitholetapiwa81@gmail.com, and lauro.tomio@unesp.br

Abstract – By studying the total fusion and breakup cross-sections in the interaction of the neutron-halo ^{11}Be projectile on the lead target ^{208}Pb , it is shown that, even for the neutron-halo projectile, the breakup channel remains the most dominant reaction channel at sub-barrier energies, following a characteristic behavior that was also previously verified for the case of the proton-halo projectile ^8B . This feature is found to emanate from the enhancement of the breakup cross-section, due to the continuum-continuum couplings coming exclusively from its Coulomb component. We further speculate that the enhancement of the Coulomb breakup cross-section at sub-barrier incident energies by the continuum-continuum couplings could be associated with the projectile breaking up on the outgoing trajectory, provided these couplings can be proven to delay the breakup process.

Introduction. – A recent experimental measurement of the breakup of ^8B proton-halo nucleus on a lead target at deep sub-barrier energies by Pakou *et al.* [1], yielded a quite interesting result: the breakup channel is reported to be the main reaction channel at these energies. Intuitively, one assumes that at deep sub-barrier energies, the reaction should be dominated by reaction channels other than the breakup channel. In a subsequent study [2], it was evidenced that the predominance of the breakup channel over the fusion channel in this incident energy region could be attributed to couplings among the continuum states of the projectile. Using the continuum discretized coupled channels (CDCC) calculations, further analysis led to the conclusion that such continuum-continuum couplings (CCC) indicate the breakup on the outgoing trajectory. While these couplings are known to suppress strongly the breakup cross-sections at incident energies above the Coulomb barrier [3–10], it was verified in Ref. [2] that they enhance the breakup cross-section at sub-barrier energies, being further argued that this enhancement could be attributed to the breakup occurring on the outgoing trajectory. However, the question remains open

whether the projectile breaks up on its incoming trajectory toward the target or on its outgoing trajectory as it leaves the target and how that affects the breakup dynamics.

A subsequent analysis in Ref. [11], of the same reaction with the ^8B proton-halo nucleus, within the same incident energy range, further confirmed the findings of Ref. [1], by indicating the effect of Coulomb polarization on the proton halo state, with the correlation information revealing that the prompt breakup mechanism dominates, occurring predominantly on the outgoing trajectory. This assertion corroborates the conclusion anticipated in Ref. [2] that the breakup of the projectile occurs in the outgoing trajectory.

Particularly, in Ref. [11], it was emphasized the relevance in elucidating the long-standing question about the breakup dynamics of a proton halo nucleus. Relying on the results obtained near Coulomb barrier energies, their analyses have signaled distinctive dynamics of a proton-halo nucleus as compared with a neutron-halo nucleus, which has been assigned to the Coulomb effect of the halo proton, indicating little influence of the continuum on elastic scattering and complete fusion. Nevertheless, as commented in Ref. [11], further investigations are still desired to elucidate the breakup behavior of a proton halo nuclear system, which can be quite rel-

(a) Author to whom any correspondence should be addressed.

evant in the light of potential astrophysical implications. In this regard, one could check whether the conclusions reported in Refs. [1, 2, 11] can be assumed as a universal signature of the breakup of weakly-bound systems at deep sub-barrier energies, by first extending the same investigation to neutron-halo projectiles. The fundamental difference between proton-halo and neutron-halo is the presence of the Coulomb barrier in the core-proton system, which is absent in the core-neutron system since the neutron is not charged. Therefore, considering a neutron-halo projectile for the same study would provide an opportunity to test, whether the importance of the breakup channel over other reaction channels at deep sub-barrier incident energies emanate from dynamical effects (associated with the projectile-target interaction), or from static effects (associated with the projectile ground-state wave function). On the competition between the breakup and fusion channels below the Coulomb barrier, it was also shown previously that the breakup cross-section becomes dominant over the fusion cross-section, in Refs. [12,13]. By assuming the same heavy target ^{208}Pb , this was shown in Ref. [12], when studying the Coulomb barrier penetrability using the ^{11}Be projectile; and, in Ref. [13], by considering the ^6Li as the projectile, treated as a weakly-bound cluster of an alpha particle with a deuteron. In short, despite the registered successes over the past decades in probing nuclear reactions by weakly-bound exotic projectiles in heavy targets, which can be traced through recent studies [14–21,40], with their cited references, these investigations at deep sub-barrier energies are still limited, as most available results in this topic are based on incident energies above and around the Coulomb barrier.

Our aim in this paper is to report an extension of the mentioned studies on proton-halo reactions [1, 2, 11], by considering a neutron-halo projectile, to probe the possible universality of previous conclusions. To this end, we study the breakup dynamics of the s -wave neutron-halo nucleus ^{11}Be on a lead target at Coulomb sub-barrier and around-barrier incident energies. The main goal is to verify whether, for deep sub-barrier incident energies, the breakup cross-section remains dominant over the total fusion cross-section as in the case of proton-halo projectiles, such that some universal characteristics can be extracted.

Brief theoretical approach. – The fundamental mathematical formulation of the CDCC (continuum discretized coupled channels) formalism, which is the theoretical approach used in this work, can be found in Ref. [22], such that we avoid giving more details here. For a more recent review of CDCC with its theoretical foundation, we have also the Ref. [23]. Within the CDCC formalism, once the total wave function is expanded on the projectile bound and bin states (whose wave functions are square-integrable), a truncated set of coupled differential equations of the radial part $\chi_\beta(R)$ of the wave function is obtained, which contains the coupling matrix elements

$$U_{\beta\beta'}^{LL'J}(R) = \langle \mathcal{Y}_\beta^{LJ}(\mathbf{r}, \boldsymbol{\Omega}_R) | U_{pt}(\mathbf{r}, \mathbf{R}) | \mathcal{Y}_{\beta'}^{L'J}(\mathbf{r}, \boldsymbol{\Omega}_R) \rangle, \quad (1)$$

where $\mathcal{Y}_\beta^{LJ}(\mathbf{r}, \boldsymbol{\Omega}_R)$, is the channel wave function that contains bound and bin wave functions, $\boldsymbol{\Omega}_R$ is the solid angle in the direction of the projectile-target center-of-mass \mathbf{R} , expressed in spherical coordinates, with L and J being the orbital and total angular momentum quantum numbers. In Eq. (1), $U_{pt}(\mathbf{r}, \mathbf{R}) = U_{ct}(\mathbf{R}_{ct}) + U_{vt}(\mathbf{R}_{vt})$, with U_{ct} , and U_{vt} , are core-target and valence-nucleon-target optical potentials, having the corresponding coordinates

$$\mathbf{R}_{ct} \equiv \mathbf{R} + \frac{1}{A_p} \mathbf{r}, \quad \mathbf{R}_{vt} \equiv \mathbf{R} - \frac{A_c}{A_p} \mathbf{r}, \quad (2)$$

where A_c and $A_p = A_c + 1$, are the core and projectile atomic mass numbers, respectively. In Eq. (1), $\beta \equiv (\alpha_b, \alpha_i)$, where α_b represents the quantum numbers that describe the projectile bound state, with α_i standing for the quantum numbers that describe the bin states, with $i = 1, 2, \dots, N_b$, where N_b is the number of bins.

The coupling matrix elements (1), can be split into couplings to and from the bound-state $U_{\alpha_b\alpha_i}^{LJ}(R)$, and couplings among the continuum states $U_{\alpha_i\alpha'_i}^{LL'J}(R)$, given by

$$\begin{aligned} U_{\alpha_b\alpha_i}^{LJ}(R) &= \langle \mathcal{Y}_{\alpha_b}^{LJ}(\mathbf{r}, \boldsymbol{\Omega}_R) | U_{pt}(\mathbf{r}, \mathbf{R}) | \mathcal{Y}_{\alpha_i}^{L'J}(\mathbf{r}, \boldsymbol{\Omega}_R) \rangle, \\ U_{\alpha_i\alpha'_i}^{LL'J}(R) &= \langle \mathcal{Y}_{\alpha_i}^{LJ}(\mathbf{r}, \boldsymbol{\Omega}_R) | U_{pt}(\mathbf{r}, \mathbf{R}) | \mathcal{Y}_{\alpha'_i}^{L'J}(\mathbf{r}, \boldsymbol{\Omega}_R) \rangle. \end{aligned} \quad (3)$$

The coupling matrix elements are evaluated subject to the boundary conditions in the asymptotic region ($R \rightarrow \infty$),

$$\chi_\beta(R) \xrightarrow{R \rightarrow \infty} \frac{i}{2} [H_{\alpha_i}^-(K_{\alpha_i}R)\delta_{\alpha_b\alpha_i} - H_{\alpha_i}^+(K_{\alpha_i}R)S_{\beta\beta'}^J(K_{\beta'})], \quad (4)$$

where $H_\beta^\pm(K_\beta R)$ are Coulomb-Hankel functions [24], and $S_{\alpha_i\alpha'_i}^J(K_{\alpha'_i})$ are the scattering S-matrix elements, with $K_{\alpha_i} = \sqrt{\frac{2\mu_{pt}(E - \varepsilon_{\alpha_i})}{\hbar^2}}$, where $\mu_{pt} = m_0 A_p A_t / (A_p + A_t)$ (m_0 is the nucleon's mass and A_t the projectile atomic mass number) is the projectile-target reduced mass, E is the incident energy, with ε_{α_i} being the bin energies.

The breakup cross-section can be directly obtained from the scattering matrix as follows [25]

$$\sigma_{\text{BU}} = \frac{\pi}{K_{\alpha_b}^2} \sum_{J\alpha_i L\alpha'_i L'} \frac{2J+1}{2j+1} |S_{\alpha_i\alpha'_i}^J(K_{\alpha'_i})|^2, \quad (5)$$

where j is the total angular momentum associated with the core-nucleon relative motion, and K_{α_b} , is the initial relative momentum, which is related to the final relative momentum K_{α_i} through the following energy conservation equation $\frac{\hbar^2 K_{\alpha_i}^2}{2\mu_{pt}} - \varepsilon_{\alpha_i} = \frac{\hbar^2 K_{\alpha_b}^2}{2\mu_{pt}} + \varepsilon_b$ (where $\varepsilon_b < 0$ is the ground-state binding energy). The total fusion cross-section can be obtained as follows:

$$\begin{aligned} \sigma_{\text{TF}} &= \sum_{J=0}^{J_{\text{max}}} \sigma_{\text{TF}}^{(J)} \\ \sigma_{\text{TF}}^{(J)} &= \frac{2\mu_{pt}}{\hbar^2 K_{\alpha_b}^2} (2J+1) \sum_{\beta\beta_i} \chi_\beta^{LJ}(R) |W_{\beta\beta'}^{LL'J}(R)| \chi_{\beta'}^{L'J}(R), \end{aligned} \quad (6)$$

where $W_{\beta\beta'}^{LL'J}(R)$ are the imaginary parts of the coupling matrix elements $V_{\beta\beta'}^{LL'J}(R)$ that contain the imaginary parts of the potential $U_{pt}(\mathbf{r}, \mathbf{R})$. Therefore, they are responsible for nuclear absorption.

Projectile-target potentials. A selection of the projectile-target potentials necessary to calculate both fusion and breakup cross-sections on the same footing can prove to be a challenging task. The main reason is the fact that both cross-sections emanate from different dynamics. Quite often in the literature, the Woods-Saxon form factor is used to model the real and imaginary parts of the potentials $U_{pt}(\mathbf{r}, \mathbf{R})$. With the coordinate definitions (2) and $n \equiv ct, vt$,

$$\begin{aligned} U_n(\mathbf{R}_n) &= V_n(\mathbf{R}_n) + iW_n(\mathbf{R}_n) \\ &= \frac{V_0^{(n)}}{1 + \exp[(\mathbf{R}_n - \mathbf{R}_0^{(n)})/a_0^{(n)}]} \\ &+ \frac{i W_0^{(n)}}{1 + \exp[(\mathbf{R}_n - \mathbf{R}_w^{(n)})/a_w^{(n)}]}, \quad n \equiv ct, vt \end{aligned} \quad (7)$$

where $V_0^{(n)}$ and $W_0^{(n)}$ are the depths of the real and imaginary parts, respectively, $R_0^{(n)} = r_0^{(n)}(A_n^{1/3} + A_t^{1/3})$ and $R_w^{(n)} = r_w^{(n)}(A_n^{1/3} + A_t^{1/3})$ are the corresponding nuclear radii, with a_{0n} and a_{wn} the respective diffuseness. The potentials (7) are used in the off-diagonal channels to couple bound to continuum and continuum to continuum channels. In the elastic scattering channel, the real and imaginary parts of the optical potential represent the expected value of $U_{pt}(\mathbf{r}, \mathbf{R})$, concerning the ground state of the projectile nucleus:

$$\begin{aligned} V_{\alpha_b \alpha_b}(\mathbf{R}) &= \int d^3\mathbf{r} |\phi_{\alpha_b}(\mathbf{r})|^2 V_{pt}(\mathbf{r}, \mathbf{R}), \\ W_{\alpha_b \alpha_b}(\mathbf{R}) &= \int d^3\mathbf{r} |\phi_{\alpha_b}(\mathbf{r})|^2 W_{pt}(\mathbf{r}, \mathbf{R}), \end{aligned} \quad (8)$$

where $\phi_{\alpha_b}(\mathbf{r})$ is the ground state wave function, and $V_{pt}(\mathbf{r}, \mathbf{R}) = V_{ct}(\mathbf{R}_{ct}) + V_{vt}(\mathbf{R}_{vt})$, $W_{pt}(\mathbf{r}, \mathbf{R}) = W_{ct}(\mathbf{R}_{ct}) + W_{vt}(\mathbf{R}_{vt})$, are the real and imaginary parts of $U_{pt}(\mathbf{r}, \mathbf{R})$. Given the longer tail of the projectile nucleus, due to its low breakup threshold, the nuclear forces are extended well beyond the barrier radius through the tails of $V_{pt}(\mathbf{r}, \mathbf{R})$ and $W_{pt}(\mathbf{r}, \mathbf{R})$. As such, $V_{\alpha_b \alpha_b}(\mathbf{R})$ will result in lowering the Coulomb barrier, whereas $W_{\alpha_b \alpha_b}(\mathbf{R})$ will exhibit a long-range absorption behavior. Consequently, the total fusion obtained with these potentials is expected to be much larger. Realistic fusion cross-sections (i.e., comparable with the experimental data) are generally obtained by considering short-range imaginary potentials. For example, in Refs. [6, 19, 26–28], strong short-range W_{ct} , W_{vt} , and W_{pt} , with parameters $W_0 = 50$ MeV, $r_w = 1.0$ and $a_w = 0.1$ fm, are adopted. However, such a choice of imaginary potentials may not be suitable in the calculations of breakup cross-sections.

Details of the numerical calculations. – Here we provide the necessary information on the breakup dynamics, by describing the internal structure of the neutron-halo projectile nucleus ^{10}Be . It is modeled as a ^{10}Be core nucleus to which a valence neutron is weakly bound

in the following s -wave configuration $^{10}\text{Be} \otimes n(2s_{\frac{1}{2}^+})$, with $\ell_0 = 0$, where ℓ_0 is the ground-state orbital angular momentum associated with the core-neutron relative motion. The binding energy of this ground state is $\varepsilon_0 = -0.504$ MeV [29]. Also, this nucleus exhibits a first excited bound-state with energy $\varepsilon_1 = -0.183$ MeV in the $p_{\frac{1}{2}^-}$ state ($\ell_0 = 1$), and a narrow resonance with energy $\varepsilon_{res} = 1.274$ MeV, in the $d_{\frac{3}{2}^+}$ continuum state.

To obtain the internal states of the ^{11}Be nucleus (i.e., bound and scattering states), the two-body Schrödinger equation is numerically solved, using the Woods-Saxon potential with both central and spin-orbit coupling components. For the numerical values of the different parameters, we assume the same ones considered in Ref. [9], which were taken from Ref. [30]. As already indicated, it is not straightforward the procedure in determining which common imaginary potentials to use in simultaneous calculations of both cross-sections. In this study, the choice of the long-range imaginary potentials was motivated by the understanding that these potentials are expected to provide realistic calculations for the breakup cross-section, but end up overestimating the total fusion cross-section. Therefore, once the breakup cross-section is found to be larger than the total fusion counterpart, this would be even more so when short-range imaginary potentials are used. This happens because short-range imaginary potentials are expected to enhance the breakup cross-section. By taken from Ref. [30], the real and imaginary parts of the core-target optical potential parameters used in the construction of the projectile-target coupling matrix elements, taken from Ref. [30], are $V_0 = 70$ MeV, $R_0 = 7.43$ MeV, $a_0 = 1.04$ MeV, $W_0 = 58.9$ MeV, $R_w = 7.19$ MeV, and $a_w = 1.0$ MeV. For the neutron-target optical potential, the global parametrization of Ref. [31], was adopted. These potentials, together with the folding potential (8), in the elastic scattering channel, extend the absorption to outside the usual region, increasing the fusion cross-section. So, we need to be mindful of the choice of imaginary potentials in the analysis of the results. To obtain fusion cross-sections that are comparable with the available experimental data (as it happens for $^{11}\text{B} + ^{209}\text{Bi}$ [32]), and test how the total fusion-cross section is overestimated of the long-range imaginary potentials, we will perform another set of calculations where we replace the long-range W_{ct} , W_{nt} and W_{pt} by the short-range ones, i.e., $W_0 = 50$ MeV, $r_w = 1.0$ MeV and $a_w = 0.1$ MeV, as in Refs. [6, 19, 26–28, 33]. However, by calculating with long- or short-range imaginary potential, our interest is to verify whether the breakup cross-section remains larger than the fusion cross-section at incident energies below the Coulomb barrier. And, if that is the case, why this happens.

For solving the coupled differential equations emanating from the projectile-target three-body Schrödinger equation, various numerical parameters were optimized to satisfy the convergence requirements. In this regard, the fol-

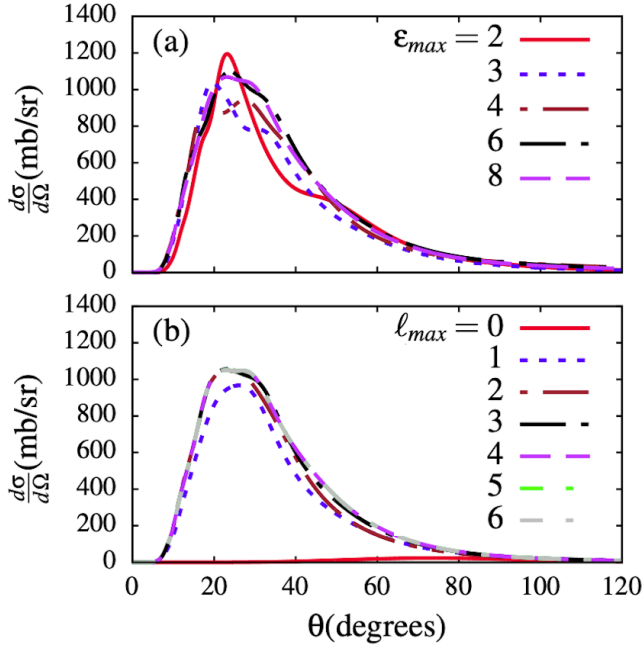


Fig. 1: Convergence results for the differential breakup cross-sections in terms of the maximum core-neutron excitation energies ε_{max} (MeV units) [panel (a)] and maximum core-neutron orbital angular momentum ℓ_{max} (\hbar units) [panel (b)].

lowing maximum limiting values were applied: For the core-neutron, the orbital angular momentum ℓ was truncated at $\ell_{max} = 6\hbar$, with $r_{max} = 100$ fm being the maximum radial coordinate r , and $\varepsilon_{max} = 8$ MeV the maximum excitation energies ε . For the projectile target, we have $L_{max} = 1000\hbar$ and $R_{max} = 500$ fm, respectively, for the maximum orbital angular momentum L and for the radial coordinate R . Also, the radial coordinates r_{max} and R_{max} were sliced into radial mesh points equally spaced by $\Delta r = 0.1$ fm and $\Delta R = 0.05$ fm, respectively. The projectile-target potentials were expanded into potential multipoles up to $\lambda_{max} = 4$. The energy interval $[0, \varepsilon_{max}]$ was discretized into energy bins of widths, $\Delta\varepsilon = 0.5$ MeV, for the s - and p -states; $\Delta\varepsilon = 1.0$ MeV, for the f - and d -states; $\Delta\varepsilon = 1.5$ MeV, for g -states; and $\Delta\varepsilon = 2.0$ MeV, for higher partial waves. Finer bins were considered for the resonant state. The numerical calculations were performed with FRESKO computer codes [24]. In Fig. 1, we show samples of convergence tests in terms of ℓ_{max} and ε_{max} for $E_{cm}/V_B = 0.8$, where $V_B = 37.90$ MeV is obtained from the São Paulo potential (SPP) [34]. As one can verify from the given results in this figure, the convergence is well reached for $\varepsilon_{max} = 8$ MeV, and $\ell_{max} = 6\hbar$.

Results and Discussion. – To further assess the stability of the numerical results and how well the experimental data can be described, we first compare in Fig. 2, the computed results for the differential breakup cross-section with the available experimental data, measured at $E_{lab} = 140$ MeV, as given in Ref. [35]. As shown, the ex-

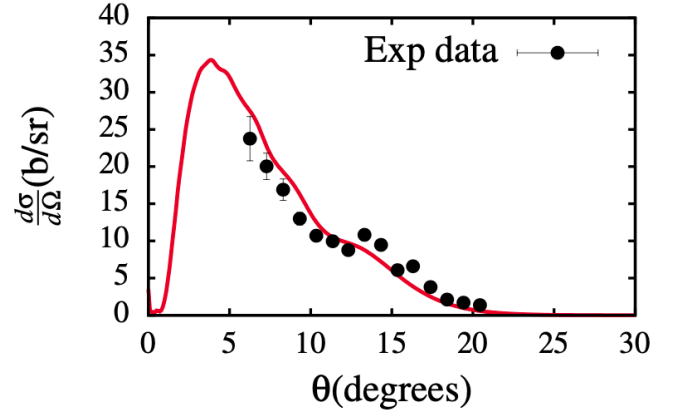


Fig. 2: Comparison of the theoretical computed breakup cross-section (solid line) with the corresponding experimental data, measured at $E_{lab} = 140$ MeV, as given in Ref. [35].

perimental data are quite well reproduced. We also found that (results not shown) the breakup cross-section with the short-range imaginary potential becomes highly oscillatory, particularly at small angles, and does not provide a good fit for the experimental data as the ones obtained with the long-range imaginary potential. This is why, as already pointed out, we chose to use the long-range imaginary potential to calculate the breakup cross-sections.

Figure 3 shows the breakup and total fusion cross-sections, respectively σ_{BU} and σ_{TF} , as functions of the ratio between total energy E_{cm} and potential barrier height V_B , with E_{cm}/V_B in the interval $[0.5, 1.3]$. The same potential parameters were applied in both calculations to obtain the breakup cross-section in Fig. 2. Although these parameters increase the total fusion cross-section, both fusion and breakup cross-sections are treated on the same footing with this choice, with the outcome not affected by different calculations. The results in Fig. 3 were obtained with all the different couplings being included in the coupling matrix elements, identified as “All coupl.,” i.e., with couplings to and from the projectile bound-state and continuum-continuum couplings. One observes that at sub-barrier energies ($E_{cm}/V_B \leq 1$), the breakup cross-section is dominant over the total fusion cross-section. The transition occurs around the Coulomb barrier where the total fusion cross-section prevails. Therefore, one can infer that, even in the case of a neutron-halo weakly-bound projectile, the breakup channel remains the dominant reaction channel at sub-barrier incident energies. It is interesting to see that even when long-range imaginary potentials are considered which are known to increase the fusion cross-section, the breakup cross-section remains more important than its fusion counterpart. In this regard, it follows that the conclusions of Refs. [1, 2, 11] on proton-halo projectile can also be extended to a neutron-halo projectile. We do not expect the use of short-range imaginary potentials to reverse this trend at sub-barrier energies, but such

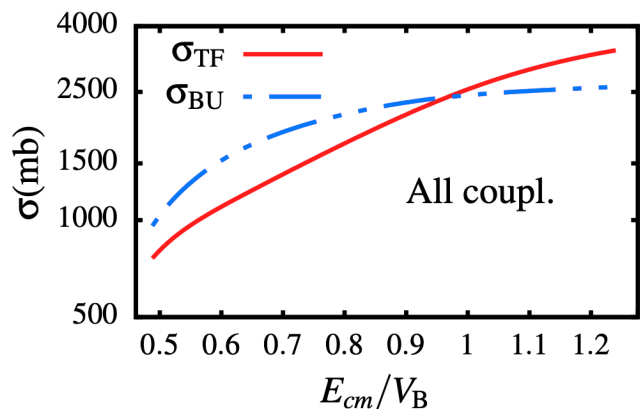


Fig. 3: Breakup (dash-dotted line) and total fusion (solid line) cross-sections, plotted as functions of the incident energy scaled by the Coulomb barrier height V_B , and obtained when all the different coupled channels are included in the coupling matrix elements.

potentials can be expected to push the transition point where the fusion cross-section becomes more important for larger incident energies. The results in Fig.3, further suggests that the Coulomb barrier in the core-proton system is not responsible for the importance of the breakup cross-section over the total fusion cross-section at sub-barrier incident energies, which implies that static effects related to the projectile ground-state wave function are not the main factor contributing to this phenomenon. As argued in Ref. [2], this leaves dynamical effects (due to the projectile-target interaction) as one of the main factors responsible for the importance of the breakup cross-section over the total fusion cross-sections at incident sub-barrier energies. A similar trend regarding the importance of the breakup cross-section over the total fusion cross-section was also reported in the breakup of ${}^6\text{Li}$ nucleus (treated as a weakly-bound cluster of an alpha particle and the deuteron) on the same target nucleus [13].

To verify how the long-range imaginary potentials overestimate the total fusion cross-section, we repeated the same calculations, but with the short-range imaginary potentials, as described in the previous section. The calculated fusion and breakup cross-sections are shown in Fig.4. Compared to Fig.3, it is noticed that the total fusion cross-sections are largely suppressed, and the breakup cross-section becomes substantially larger than the fusion cross-section. Although the fusion cross-sections, as shown in Fig.4, are not considered in the following discussion, we are aware of this suppression. Within a careful comparison, the Figs.3 and 4 suggest that the difference between both breakup cross-sections is not very pronounced. However, one can verify that the results obtained with short-range imaginary potentials are significantly larger than those obtained with long-range imaginary potentials.

To gain more insight into the importance of the breakup cross-section over the total fusion cross-section at sub-

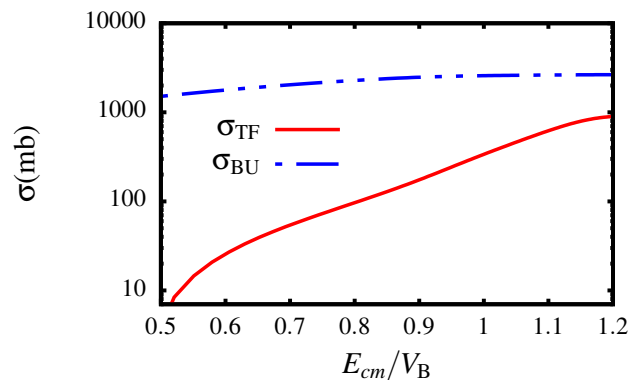


Fig. 4: Fusion and breakup cross-section as a function of E_{cm}/V_B , obtained when the long-range imaginary part of the nuclear potential is replaced by the short-range one, i.e., with $W_0 = 50$ MeV, $r_w = 1.0$ MeV and $a_w = 0.1$ MeV for core-target, neutron-target and projectile-target imaginary potentials.

barrier energies, it is essential to investigate the effect of the continuum-continuum couplings. In Fig.5, we compare the total fusion and breakup cross-sections obtained when the continuum-continuum couplings are removed from the coupling matrix elements (without CCC), i.e., leaving a single transition to and from the projectile bound state. By inspecting the results shown in that figure a stark difference from Fig. 3 is observed (with all couplings), as one notes that, at sub-barrier energies ($E_{cm}/V_B \leq 0.8$), both breakup and total fusion cross-sections are almost similar, with the two curves becoming hardly distinguishable. Above the Coulomb barrier, the breakup cross-section starts becoming dominant. So, by comparing Figs.3 and 5, the continuum-continuum couplings appear to be responsible for the quantitative importance of the breakup cross-section over the fusion cross-section at sub-barrier incident energies, as also previously reported in Ref. [2]. However, considering the fusion calculations as given in Fig.4, with short-range imaginary part in the nuclear potential, the fusion cross-section in the absence of the continuum-continuum couplings would be lower than the breakup cross-section even at sub-barrier energies. Therefore, although Fig. 5 does not provide a realistic picture, it points out the fact that when the continuum-continuum couplings are removed from the matrix elements, the gap between the two curves will be significantly narrowed.

To better assess of the significance of the continuum-continuum couplings on the breakup cross-section, we plot in Fig. 6, the breakup cross-sections in the presence and absence of the continuum-continuum couplings. Observing that figure, it resorts that at deep sub-barrier energies ($E_{cm}/V_B \leq 0.7$), the continuum-continuum couplings serve to enhance the breakup cross-section, as the breakup cross-section in the presence of these couplings is larger than the breakup cross-section in the absence of these couplings. A similar trend is reported in Ref. [10], in the case of the breakup of the weakly-bound cluster system ${}^6\text{Li}$

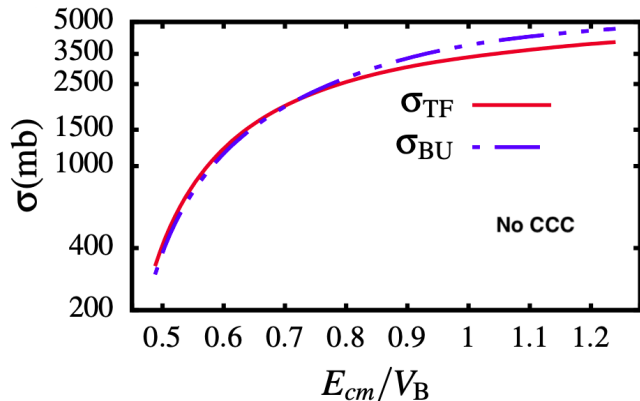


Fig. 5: Breakup and total fusion cross-sections as functions of the incident energy scaled by the Coulomb barrier height V_B , and obtained when the continuum-continuum couplings are excluded (“No CCC”) from the coupling matrix elements.

on the same target nucleus. At larger incident energies ($E_{cm}/V_B > 0.7$), the continuum-continuum couplings account for the suppression of the breakup cross-section.

What can we learn from the enhancement of the breakup cross-section at sub-barrier energies? Notice that, according to Refs. [36, 37], the structure of the continuum, with existing resonances, may delay the breakup process. For instance, as stated in Ref. [37], “*The near-target breakup is consistent with simulations which assume that the populated continuum states have a short but finite mean life, delaying into fragments.*” The same authors further argue that: “*Similar behavior should be expected from breakup occurring from very short-lived states, irrespective of whether the breakup is direct or triggered by transfer of nucleons.*”

If it could also be verified that continuum-continuum couplings produce similar effect, then, for energies above the Coulomb barrier, delaying the breakup would mean increasing the probability of the breakup to occur within the interaction region where nuclear forces are active to trigger absorption. Therefore, at such incident energies higher than the barrier, this will lead to total fusion larger than the breakup cross-sections as verified in Fig. 3. In the same energy region, if the breakup becomes more prompt when the continuum-continuum couplings are removed, then the projectile fragments have enough time to survive absorption after the breakup, explaining the increase of the breakup cross-section over the total fusion cross-section as observed in Fig. 5. However, until it is proven that continuum-continuum couplings in fact will delay the breakup process, our assertion here remains speculative. A study in this regard could be important, by considering for example a dynamical time-dependent approach.

At sub-barrier incident energies, having low kinetic energy, the projectile further slows down due to the Coulomb repulsion. The dissipation of the projectile kinetic energy can be exacerbated by including couplings among contin-

uum, since energies are required to excite these states. As such, as an intermediate step, the projectile can be in a continuum state, although asymptotically it ends up bound. However, on the outgoing trajectory, the projectile gains an initial kinetic energy as it leaves the target, considering the fact that in that case it is accelerated by the projectile-target Coulomb force. On both incoming and outgoing projectile trajectories, the continuum-continuum couplings play the same role in the breakup process. Again, assuming that the continuum-continuum couplings could delay the breakup, then such “delay” together with the projectile acceleration coming from the projectile-target Coulomb interaction, can increase the probability of the projectile breakup on its outgoing trajectory away from the absorption region, i.e., out of reach of nuclear forces. Consequently, the fusion cross-section would be reduced at the expense of the breakup cross-section, with less amount of flux being removed from the breakup channel to feed up the fusion channel. The opposing effect of the Coulomb interaction on both incoming and outgoing trajectories is also invoked in Ref. [11] to explain the magnitude of the opening angle of the breakup fragments, considering that this angle distribution provides information on the breakup location (as shown in Ref. [38]). Therefore, we cautiously speculate that the enhancement of the breakup cross-section at sub-barrier incident energies by the continuum-continuum couplings could be associated with the breakup of the projectile occurring in the outgoing trajectory. Although it is not possible to unambiguously prove this point in this work, it could provide hints for further studies in this direction. More discussion on this aspect can be found in Refs. [11, 39].

The argument “on the outgoing trajectory the projectile can break up away from the reach of the nuclear forces” can be substantiated by showing that, at sub-barrier energies, the enhancement of the breakup cross-section is due to its Coulomb breakup component. This inference is born out of the fact that on the outgoing trajectory the nuclear breakup becomes increasingly less relevant as the projectile moves away from the target nucleus. To shed more light on this, let us analyze the Coulomb and nuclear breakup cross-sections.

Notice that the breakup cross-section that we have so far discussed is obtained by coherently including both Coulomb and nuclear interactions in the coupling matrix elements, this we also call total (Coulomb + nuclear) breakup cross-section. The separation of the total breakup cross-section into its Coulomb and nuclear components is not a straightforward task, and this work is not intended to perform such a task. To obtain the Coulomb and nuclear breakup cross-sections, we resort to the following approximate procedure. To calculate the Coulomb breakup cross-section, we removed all the core-target and neutron-target nuclear interactions from the coupling matrix elements, keeping only its monopole component in the elastic scattering channel. This potential (as in all other calculations), was obtained by folding the projectile

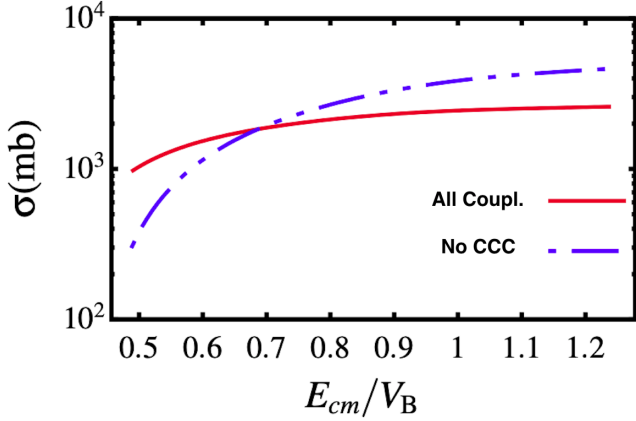


Fig. 6: Breakup cross-sections plotted as functions of the incident energy scaled by the Coulomb barrier height V_B , and obtained when all the different couplings are included in the coupling matrix elements “All coupl.” and when the continuum-continuum couplings are excluded from the couplings matrix elements “No CCC”.

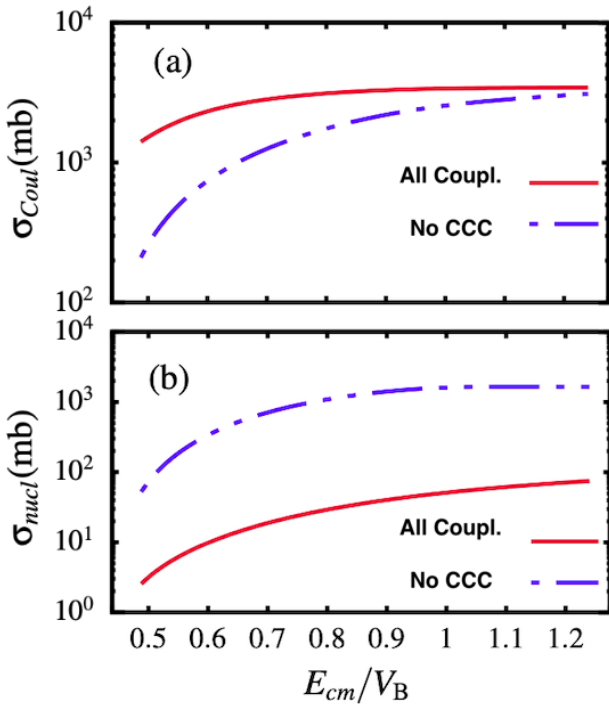


Fig. 7: Coulomb breakup cross-sections [panel (a)] and nuclear breakup cross-sections [panel (b)] plotted as functions of the incident energy scaled by the Coulomb barrier height V_B , and obtained when the continuum-continuum couplings are included and excluded from the coupling matrix elements.

ground-state density with the projectile-target potentials. In this case, the Coulomb breakup cross-section is affected by the absorption in the elastic scattering channel due to the imaginary component of this potential. Similarly, the nuclear breakup cross-sections were obtained by removing

the core-target Coulomb potential from the coupling matrix elements, also keeping its monopole diagonal term in the elastic scattering channel. This approach, although approximate, has proven to yield the desired effect.

The Coulomb and nuclear breakup cross-sections thus obtained are shown in Fig.7. Indeed, in that figure, we notice that at sub-barrier energies, the Coulomb breakup cross-section is strongly enhanced by the continuum-continuum couplings [see panel (a)]. As the incident energy increases, the enhancement strength decreases and the trend suggests that at higher incident energies, the continuum-continuum couplings would amount to a smaller effect on the Coulomb breakup cross-section. In fact, it has been shown that at higher incident energy, these couplings have very small suppression effect on the Coulomb breakup cross-section (see for example Ref. [9]). In contrast, panel (b) of Fig.7 shows that the nuclear breakup cross-section is strongly suppressed by continuum-continuum couplings at all the displayed incident energy regions. At energies above the barrier, the nuclear breakup cross-section is known to be strongly suppressed by these couplings compared to the Coulomb breakup cross-section. In fact, in Ref. [9], this suppression is reported as one of the main reasons why the Coulomb breakup is more important than the nuclear breakup in reactions involving heavy targets. Comparing the effect of the continuum-continuum couplings on Coulomb and nuclear breakup cross-sections, it follows that the enhancement of the total breakup cross-section at sub-barrier incident energies due to these couplings comes exclusively from the Coulomb breakup.

Conclusion. – In this paper, we have analyzed the breakup of the weakly-bound neutron-halo nucleus ^{11}Be on a lead target at the sub-barrier and around the barrier incident energies. It is found that at deep sub-barrier energies, the breakup cross-section is dominant over the total fusion cross-section, implying that it is the leading reaction channel at this incident energy range, as also reported in the case of the proton-halo projectile ^8B on the same target. The continuum-continuum couplings, which are reported to enhance the breakup cross-section at sub-barrier energies, are found to be responsible for this feature. The enhancement of the breakup cross-section by these couplings, at sub-barrier energies, is found to come exclusively from its Coulomb component. Based on this, we are speculating that such enhancement of the Coulomb breakup cross-section by the continuum-continuum couplings could be associated with the breakup occurring on the outgoing trajectory, provided it is proven that these couplings delay the breakup process.

In summary, our study is confirming that the importance of the breakup channel over the total fusion channel, at energies below the Coulomb barrier, can also be extended to neutron-halo projectile on heavy targets. In spite of the fact that a detailed study may be required, based on the available investigations, one can anticipate

this conclusion as being a universal feature in the breakup of weakly bound projectiles on heavy targets.

* * *

We acknowledge partial support from the Brazilian agency Conselho Nacional de Desenvolvimento Científico e Tecnológico [INCT-FNA Proc. 464898/2014-5 (BM, LT) and Proc. 304469/2019-0(LT)].

REFERENCES

- [1] PAKOU A. *et al.*, *Phys. Rev. C*, **102** (2020) 031601(R).
- [2] MUKERU B., NDALA L. V. and LEKALA M. L., *Pramana J. Phys.*, **95** (2021) 106.
- [3] NUNES F. M. and THOMPSON I. J., *Phys. Rev.*, **59** (1999) 2652-2659.
- [4] SUMMERS N. C. and NUNES F. M., *Phys. Rev. C*, **70** (2004) 011602(R).
- [5] CANTO L. F., LUBIAN J., GOMES P. R. S. and HUSSEIN M. S., *Phys. Rev. C*, **80** (2009) 047601.
- [6] DIAZ-TORRES A. and THOMPSON I. J., *Phys. Rev. C*, **65** (2002) 024606.
- [7] MUKERU B., *J. Phys. G: Nucl. Part. Phys.*, **45** (2018) 065201.
- [8] MUKERU B., LEKALA M. L. and DENIKIN A. S., *Nucl. Phys. A*, **935** (2015) 18.
- [9] MUKERU B. and TOMIO L., *Chin. Phys. C*, **46** (2022) 014103.
- [10] MUKERU B., RAMPHO G. J. and LEKALA M. L., *J. Phys. G: Nucl. Part. Phys.*, **45** (2018) 045101.
- [11] YANG L. *et al.*, *Nature Communications*, **13** (2022) 7193.
- [12] MUKERU B., LEKALA M. L. and RAMPHO G. J., *J. Phys. G: Nucl. Part. Phys.*, **42** (2015) 085110.
- [13] OTOMAR D. R., GOMES P. R. S., LUBIAN J., CANTO L. F. and HUSSEIN M. S., *Phys. Rev. C*, **87** (2013) 014615.
- [14] LHA V., PARKAR V. V. and KAILAS S., *Phys. Rep.*, **845** (2020) 1.
- [15] CANTO L. F., GUIMARÃES V., LUBIAN J. and HUSSEIN M. S., *Eur. Phys. J. A*, **56** (2020) 281.
- [16] MUKERU B., FREDERICO T. and TOMIO L., *Phys. Rev. C*, **102** (2022) 064623.
- [17] WANG K. *et al.*, *Phys. Rev. C*, **103** (2021) 024606.
- [18] PIETRO A. D. *et al.*, *J. Phys.: Conf. Ser.*, **2586** (2023) 012079.
- [19] FERREIRA J. L., RANGEL J., LUBIAN J. and CANTO L. F., *Phys. Rev. C*, **107** (2023) 034603.
- [20] MUKERU B., *EPL*, **143** (2023) 64003.
- [21] MUKERU B., MAHATIKELE M. B. and RAMPHO G. J., *Phys. Rev. C*, **107** (2023) 064313.
- [22] AUSTERN N., ISERI Y., KAMIMURA M., KAWAI M., RAWITSCHER G. and YAHIRO M., *Phys. Rep.*, **154** (1987) 125.
- [23] YAHIRO M., OGATA K., MATSUMOTO T. and MINOMO K., *Prog. Theor. Exp. Phys.*, **2012** (2012) 01A206.
- [24] THOMPSON I. J., *Comp. Phys. Rep.*, **7** (1988) 167.
- [25] DESCOUVEMONT P., CANTO L. F. and HUSSEIN M. S., *Phys. Rev. C*, **95** (2017) 014604.
- [26] HAGINO K., VITTURI A., DASSO C. H. AND LENZI S. M., *Phys. Rev. C*, **61** (2000) 037602.
- [27] LUBIAN J., FERREIRA J. L., RANGEL J., CORTES M. R. AND CANTO L. F., *Phys. Rev. C*, **105** (2022) 054601.
- [28] GÓMEZ CAMACHO A., WANG B. and ZHANG H. Q., *Phys. Rev. C*, **97** (2018) 054610.
- [29] WANG M. *et al.*, *Chin. Phys. C*, **41** (2017) 030003.
- [30] CAPEL P., BAYE D. and MELEZHIK V. S., *Phys. Rev. C*, **68** (2003) 014612.
- [31] KONING A. J., and DELAROCHE J. P., *Nucl. Phys. A*, **713** (2003) 231.
- [32] HINDE D. J. AND DASGUPTA M., *Phys. Rev. C*, **81** (2010) 064611.
- [33] SIGNORINI C. *et al.*, *Nucl. Phys. A*, **753** (2004) 329.
- [34] CHAMON L. C. *et al.*, *Phys. Rev. C*, **66** (2002) 014610.
- [35] DUAN F. F. *et al.*, *Phys. Lett. B*, **811** (2020) 135942.
- [36] DIAS-TORRES A. AND QURAIISHI D., *Phys. Rev. C*, **97** (2018) 024611.
- [37] KALKAL S. *et al.*, *Phys. Rev. C*, **93** (2016) 044605.
- [38] SIMPSON E. C. *et al.*, *Phys. Rev. C*, **93** (2016) 024605.
- [39] ZHANG H., *Science Bulletin*, **68** (2023) 2.
- [40] RANGEL J. *et al.*, *Phys. Lett. B*, **803** (2020) 135337.